



Sonja Tötz | Jakob Löber | Jan Frederik Tötz | Harald Engel

# Control of transversal instabilities in reaction-diffusion systems

Suggested citation referring to the original publication:

New Journal of Physics 20 (2018) 053034

DOI <https://doi.org/10.1088/1367-2630/aabce5>

ISSN (online) 1367-2630

Postprint archived at the Institutional Repository of the Potsdam University in:

Postprints der Universität Potsdam

Mathematisch-Naturwissenschaftliche Reihe ; 962

ISSN 1866-8372

<https://nbn-resolving.org/urn:nbn:de:kobv:517-opus4-469762>

DOI <https://doi.org/10.25932/publishup-46976>





## PAPER

**Control of transversal instabilities in reaction-diffusion systems**

## OPEN ACCESS

## RECEIVED

24 December 2017

## REVISED

1 April 2018

## ACCEPTED FOR PUBLICATION

10 April 2018

## PUBLISHED

11 May 2018

Original content from this work may be used under the terms of the [Creative Commons Attribution 3.0 licence](#).

Any further distribution of this work must maintain attribution to the author(s) and the title of the work, journal citation and DOI.

**Sonja Totz<sup>1,2</sup>, Jakob Löber<sup>3,4</sup>, Jan Frederik Totz<sup>4,5</sup>  and Harald Engel<sup>4</sup>**<sup>1</sup> Potsdam Institute for Climate Impact Research, Telegrafenberg A61, D-14473 Potsdam, Germany<sup>2</sup> Department of Physics, University of Potsdam, Karl-Liebknecht-Straße 24/25, D-14476 Potsdam, Germany<sup>3</sup> Max-Planck-Institut für Physik komplexer Systeme, Nöthnitzer Straße 38, D-01187 Dresden, Germany<sup>4</sup> Institut für Theoretische Physik, EW 7-1, Hardenbergstraße 36, Technische Universität Berlin, D-10623 Berlin, Germany<sup>5</sup> Author to whom any correspondence should be addressed.E-mail: [sonja.totz@pik-potsdam.de](mailto:sonja.totz@pik-potsdam.de), [jakob@physik.tu-berlin.de](mailto:jakob@physik.tu-berlin.de), [jantotz@itp.tu-berlin.de](mailto:jantotz@itp.tu-berlin.de) and [h.engel@physik.tu-berlin.de](mailto:h.engel@physik.tu-berlin.de)**Keywords:** traveling waves, control, transversal instabilitiesSupplementary material for this article is available [online](#)**Abstract**

In two-dimensional reaction-diffusion systems, local curvature perturbations on traveling waves are typically damped out and vanish. However, if the inhibitor diffuses much faster than the activator, transversal instabilities can arise, leading from flat to folded, spatio-temporally modulated waves and to spreading spiral turbulence. Here, we propose a scheme to induce or inhibit these instabilities via a spatio-temporal feedback loop. In a piecewise-linear version of the FitzHugh–Nagumo model, transversal instabilities and spiral turbulence in the uncontrolled system are shown to be suppressed in the presence of control, thereby stabilizing plane wave propagation. Conversely, in numerical simulations with the modified Oregonator model for the photosensitive Belousov–Zhabotinsky reaction, which does not exhibit transversal instabilities on its own, we demonstrate the feasibility of inducing transversal instabilities and study the emerging wave patterns in a well-controlled manner.

**1. Introduction**

A large variety of pattern forming processes can be understood in terms of the advancement of an interface between two or more spatial domains. An interface that becomes unstable to diffusion may cause intricate spatio-temporal dynamics. Well-known examples include the Mullins–Sekerka instability during crystal growth and formation of snow flakes [1–3], and the Saffman–Taylor instability leading to viscous fingering in multiphase flow and porous media [4–6]. Other phenomena affected by interfacial instabilities are flame fronts [7, 8], Marangoni convection [9], and growing cell monolayers [10].

Traveling plane waves in excitable media exhibit interfacial instabilities as well. Here, an effective interface separates the excited state from the excitable rest state. A straight iso-concentration line of a two-dimensional flat wave can suffer an instability leading to stationary or time dependent modulations orthogonal to the propagation direction. Further away from the instability threshold, rotating wave segments and spreading spiral turbulence are observed [11, 12]. For standard activator–inhibitor kinetics, these so-called transversal or lateral wave instabilities typically occur if the inhibitor diffuses much faster than the activator. This result was analytically predicted first by Kuramoto for piecewise-linear reaction kinetics [13, 14]. Later, it was confirmed numerically by Horváth *et al* for autocatalytic reaction-diffusion fronts with cubic reaction kinetics [15] as well as in experiments with the iodate–arsenous acid reaction [16] and the acid-catalyzed chlorite–tetrathionate reaction [17].

A well-established system for studying chemical pattern formation, the Belousov–Zhabotinsky (BZ) reaction [18], does typically not display transversal wave instabilities. Dispersing the reagents of the BZ reaction in nanodroplets of a water-in-oil emulsion allows one to increase the inhibitor diffusivity considerably and leads, for example, to Turing patterns as reported by Vanag and Epstein [19]. Even in the presence of an electrical field that enhances transversal instabilities in cubic autocatalytic reaction-diffusion fronts, the inhibitor diffusion coefficient is always required to be larger than that of the activator [20–22].

The photosensitive BZ reaction (PBZR) is well-suited for experiments, due to the possibility of applying spatio-temporal external forcing or feedback-mediated control by exploiting the dependence of the local excitation threshold on the intensity of applied illumination [23]. Planar wave deformations due to modulated substrate height were mitigated by stationary localized light application [24]. Feedback loops were used to stabilize unstable wave segments and to guide their propagation along pre-determined trajectories [25, 26]. Also, spiral wave drift in response to resonant external forcing and various feedback-mediated control loops have been extensively studied experimentally in PBZR systems, compare for example [27–31].

In this paper, we design a curvature-dependent spatio-temporal feedback loop in order to control transversal instabilities. First, we investigate the piecewise linear FitzHugh–Nagumo (FHN) model under conditions where planar wave propagation fails due to transversal instabilities. We suppress the ongoing break-up and segmentation of waves using the feedback mechanism, thereby stabilizing unstable propagating planar waves. Second, as a model for the experimentally relevant PBZR, we analyze the modified Oregonator model which does not exhibit transversal instabilities in the parameter regime relevant for experiments. We destabilize a stable propagating planar reaction-diffusion wave by inducing transversal instabilities via feedback, and study the wave patterns emerging beyond the instability threshold. In addition we demonstrate the capability to actively select wave patterns by modifying feedback parameters accessible in a chemical experiment.

## 2. Suppression of transversal instabilities

### 2.1. The piecewise-linear FHN model

The piecewise-linear caricature of the FHN model [12, 32] received some attention in the context of transversal instabilities [12]. It is a two component model of standard activator-inhibitor type,

$$\frac{\partial u}{\partial t} = \Delta u + F(u, v), \quad (1)$$

$$\frac{\partial v}{\partial t} = \sigma \Delta v + \epsilon G(u, v), \quad (2)$$

with  $u$  being the activator and  $v$  the inhibitor. The reaction kinetics are a piecewise-linear caricature of the FHN model

$$F(u, v) = f(u) - v, \quad (3)$$

$$G(u, v) = k_g u - v, \quad (4)$$

where

$$f(u) = \begin{cases} -k_1 u, & u < \delta, \\ k_f(u - a), & \delta < u < 1 - \delta, \\ k_2(1 - u), & 1 - \delta < u. \end{cases} \quad (5)$$

The parameters  $k_1$  and  $k_2$  are chosen such that  $f(u)$  is continuous at  $u = \delta$  and  $u = 1 - \delta$ , which leads to

$$k_1 = \frac{k_f}{\delta}(a - \delta), \quad k_2 = \frac{k_f}{\delta}(1 - \delta - a). \quad (6)$$

The remaining parameters for the function  $f$  are chosen in such a way that  $f$  resembles the cubic shape of the FHN activator nullcline. All parameter values used in numerical simulations are listed in table A1 in appendix A. The parameter  $a$  is a measure for the excitation threshold and used as the feedback parameter.

For numerical simulations, we assume an elongated two-dimensional channel of width  $L$  in the  $y$ -direction with waves propagating in the  $x$ -direction. The boundary conditions in the  $x$ -direction are periodic while we assume Neumann boundary conditions in the  $y$ -direction. We use an arc-like initial condition of width  $b$  for the vector of components  $\mathbf{u}$ ,

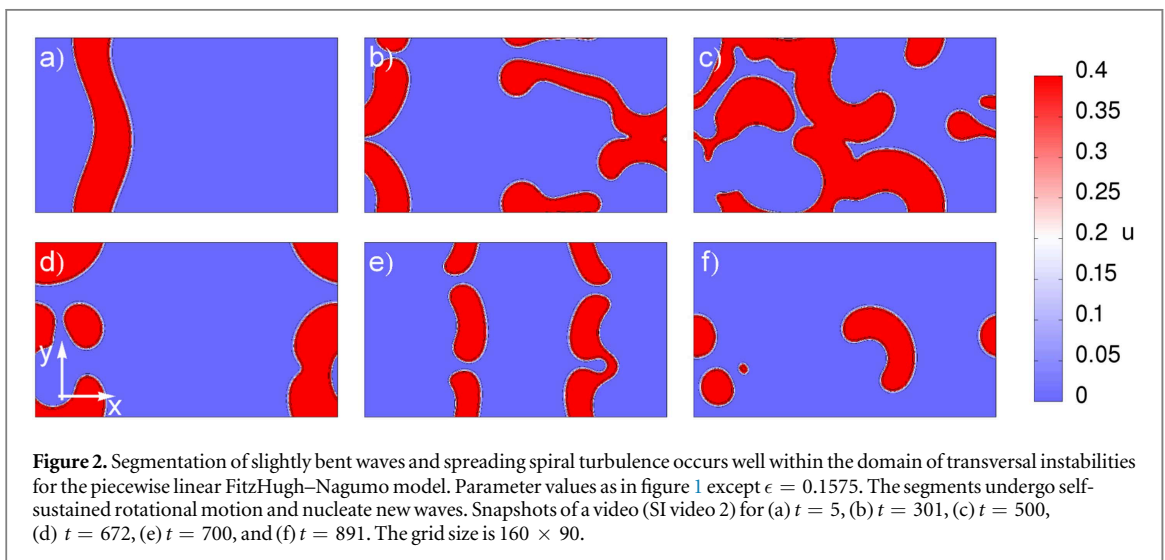
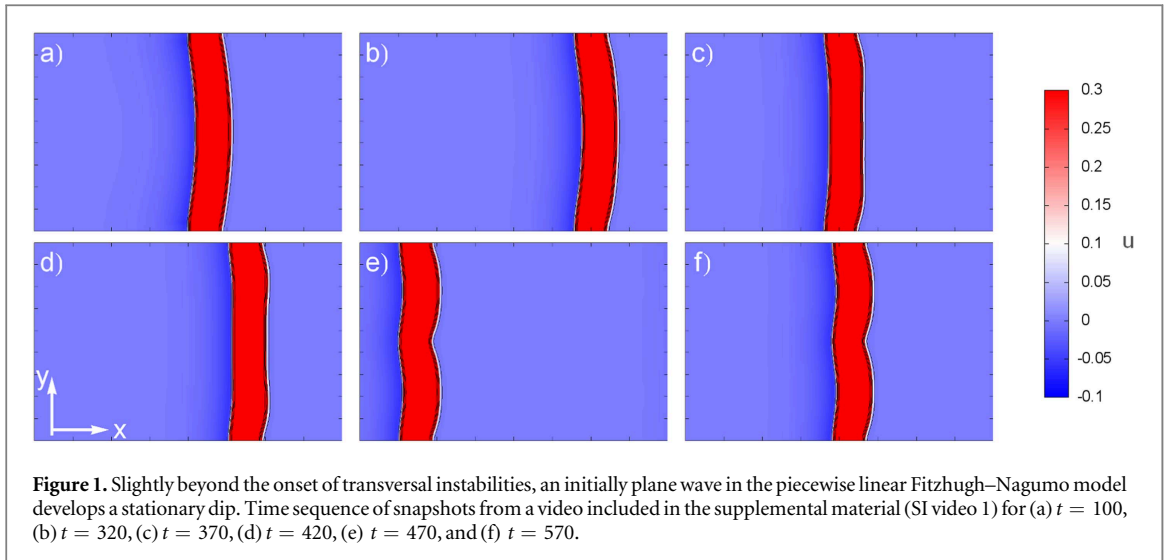
$$\mathbf{u}(x, y, t_0) = \Theta_{\text{Box}}((x - \phi(y, t_0))/b)(\mathbf{u}_{\text{max}} - \mathbf{u}_0) + \mathbf{u}_0, \quad (7)$$

where  $\mathbf{u}_{\text{max}}$  is the initial height of the pulse and  $\mathbf{u}_0$  is the stationary point of the reaction kinetics. The box function is defined as

$$\Theta_{\text{Box}}(x) = \begin{cases} 1, & |x| < 1/2, \\ 0, & |x| \geq 1/2. \end{cases} \quad (8)$$

The initial shape of the wave is given by

$$\phi(y, t_0) = d - A \cos\left(\frac{2\pi y}{L}\right), \quad (9)$$



where  $A$  denotes the amplitude of deviation of the shape from a plane wave and  $d$  is an offset. For numerical simulations in two spatial dimensions, we use a forward Euler scheme for the time evolution and a five point stencil for the Laplacian [33].

A phase diagram for the occurrence of transversal instabilities in the  $\epsilon$ - $\sigma$ -parameter plane of the piecewise-linear FHN model was presented by Zykov *et al* in [12]. Increasing the inhibitor diffusion coefficient  $\sigma$  crosses the threshold for transversal instabilities. Shortly beyond the onset of transversal instabilities, a plane wave develops a dip which is stationary in a co-moving frame of reference, see figure 1 for a time sequence of snapshots and the supplemental material for a movie (SI video 1 is available online at [stacks.iop.org/NJP/20/053034/mmedia](https://stacks.iop.org/NJP/20/053034/mmedia)). Further away from the instability threshold, a plane wave breaks into segments, which undergo self-sustained rotational motion accompanied by permanent merging and annihilation of segments. This regime is also known as spreading spiral turbulence [12], see figure 2 for a time sequence of snapshots and the supplemental material for a movie (SI video 2).

## 2.2. The eikonal equation

Theoretically the onset of transversal instabilities can be understood with the linear eikonal equation

$$c_n(s, t) = c - \nu\kappa(s, t), \quad (10)$$

an evolution equation for a two-dimensional curve  $\gamma(s, t) = (\gamma_x(s, t), \gamma_y(s, t))^T$  representing an iso-concentration line parametrized by the curve arclength  $s$ . The linear eikonal equation relates the normal velocity  $c_n$  along  $\gamma$ ,

$$c_n(s, t) = \mathbf{n}(s, t) \cdot \partial_t \gamma(s, t), \quad (11)$$

linearly to its curvature,

$$\kappa(s, t) = \frac{\partial_s \gamma_x(s, t) \partial_s^2 \gamma_y(s, t) - \partial_s \gamma_y(s, t) \partial_s^2 \gamma_x(s, t)}{((\partial_s \gamma_x(s, t))^2 + (\partial_s \gamma_y(s, t))^2)^{3/2}}, \quad (12)$$

where  $\mathbf{n}$  is the normal vector of  $\gamma$ . The curvature is conventionally assumed to be positive for convex iso-concentration lines, i.e., an iso-concentration line with a bulge in the propagation direction. The constant  $c$  corresponds to the pulse velocity of a one-dimensional solitary wave and  $\nu$  is the curvature coefficient. A rigorous derivation of the eikonal equation (10) from the reaction-diffusion system identifies the constant  $\nu$  in terms of the one-dimensional pulse profile, its response function and the matrix of diffusion coefficients, see [34] for details. For a plane wave, any iso-concentration level is a straight line and therefore its curvature vanishes,  $\kappa(s, t) \equiv 0$ , everywhere along  $\gamma$ . The stability of a plane wave is determined by the sign of the curvature coefficient  $\nu$ . As long as  $\nu > 0$ , any point along the iso-concentration line of a convex bulge moves slower than a plane wave. Points along a concave dent move faster than a plane wave, thereby smoothing out deviations from a plane wave. If  $\nu < 0$ , a convex bulge moves faster than a plane wave, protruding the bulge even further and thereby leading to an ever increasing curvature: a transversal instability arises. Patterns arising for  $\nu < 0$  cannot be described by the linear eikonal equation and terms depending nonlinearly on the curvature have to be taken into account which saturate the growth of an ever increasing curvature. At least two different nonlinear versions of equation (10) exist in the literature. Zykov *et al* [32, 35–37] renormalize  $\epsilon$  and  $\sigma$  in equation (2) to derive a one-dimensional velocity  $c$  depending on the curvature. Dierckx *et al* [34] derive higher order nonlinear corrections in the curvature by a rigorous perturbation expansion with a small parameter proportional to the curvature, additionally generalizing the eikonal equation to anisotropic media.

### 2.3. Curvature-dependent feedback control

The feedback scheme proposed in this article requires that the velocity  $c$  of a one-dimensional wave depends sufficiently strong on a parameter  $a$  which is accessible in numerical or real-world experiments. First, we linearly approximate relationship between velocity and excitation threshold as

$$c(a) = c_0 + c_1 a. \quad (13)$$

Second, we propose a feedback scheme for  $a$  depending linearly on the curvature,

$$a(\kappa) = \alpha + \beta \kappa. \quad (14)$$

The parameters  $\alpha$  and  $\beta$  are accessible to an experimentalist. In general, these parameters can be adjusted with time to achieve a better performance of the control. Together with equations (14) and (37), the linear eikonal equation (10) becomes

$$c_n = c_0 + c_1 \alpha - \tilde{\nu} \kappa, \quad (15)$$

with the effective curvature coefficient

$$\tilde{\nu} = \nu - c_1 \beta. \quad (16)$$

Depending on the sign of  $\tilde{\nu}$ , the control has very different effects. If a plane wave is stable with respect to transversal perturbations because  $\nu > 0$ , we can excite transversal instabilities if  $\tilde{\nu} = \nu - c_1 \beta < 0$ . Conversely, if  $\nu > 0$  such that plane waves are unstable with respect to transversal modulations, patterns can be stabilized if  $\tilde{\nu} = \nu - c_1 \beta > 0$ . An appropriate choice of the parameters  $\alpha$  and  $\beta$  in the feedback scheme (14) allows for fine control over transversal instabilities.

For the piecewise linear FHN model equations (1)–(6), the excitation threshold  $a$  is used as the feedback parameter. The approximately linear relation between plane wave velocity  $c$  and  $a$  yields equation (15) with  $c_0 = 2.23$  and  $c_1 = -8.75$ . We use a slightly modified form of the feedback law equation (14)

$$a(\kappa) = \begin{cases} a_{\min} + \beta(t) \kappa, & \kappa \geq 0, \\ a_{\min} & \kappa < 0. \end{cases} \quad (17)$$

Solitary pulses exist only for a certain range  $a \in [a_{\min}, a_{\max}]$  of  $a$  values. The coefficient  $\beta(t)$  in equation (17) is adjusted in time such that the maximum value of  $a(\kappa)$  along the iso-concentration line does not exceed or undershoot the range of existence of solitary pulses. Every 100 time steps, we determine the maximum curvature  $\kappa_{\max}(t)$  along the iso-concentration line and set  $\kappa_{\max}$  to this value,

$$\beta(t) = \frac{a_{\max} - a_{\min}}{\kappa_{\max}(t)}. \quad (18)$$

The background value of  $a$  is set to  $a_0 = 0.1$  everywhere before the feedback control is switched on at time  $t_{\text{on}}$ . To apply the feedback scheme (17) it is necessary to compute the curvature of an iso-concentration line of a chosen component with sufficient accuracy. This raises considerable difficulties.

## 2.4. Computation of curvature via level set methods

The curvature  $\kappa(s, t)$  of an iso-concentration line  $\gamma(s, t)$ , equation (12), is proportional to the second derivative of the iso-concentration line with respect to the curve arclength  $s$ . Computations of iso-concentration lines in numerical simulations or experiments are affected by noise due to the discretized nature of the computed or measured concentration field  $u$ . Numerical differentiation is an ill-posed mathematical operation and typically amplifies noise. A variety of methods to compute the curvature  $\kappa$  directly from a numerically determined iso-concentration line were tested and discarded due to insufficient performance [38].

An indirect method which avoids the differentiation of an iso-concentration line is to compute the curvature field  $\tilde{\kappa}$  as

$$\tilde{\kappa}(\mathbf{r}, t) = \nabla \cdot \frac{\nabla u(\mathbf{r}, t)}{|\nabla u(\mathbf{r}, t)|}. \quad (19)$$

According to the formula of Bonnet [39], evaluating  $\tilde{\kappa}$  at an iso-concentration line  $\mathbf{r} = \gamma(s, t)$  of  $u$  yields the curvature  $\kappa$  of  $\gamma$ ,

$$\kappa(s, t) = \tilde{\kappa}(\gamma(s, t), t). \quad (20)$$

See appendix B for a proof of Bonnet's formula. Equation (19) involves the determination of the second derivative of  $u$  with respect to  $x$  and  $y$ . These expressions are readily available from the finite difference algorithm used to solve the RD system numerically. The problem is now that the concentration  $u$  of a pulse solution typically varies very fast in a small spatial region while it is constant everywhere else, leading to an ill-defined denominator in equation (19). This difficulty can be addressed with the help of the level set method [40], which, however, is numerically quite expensive.

Originally, level set methods were developed by Osher and Sethian to compute and track the motion of interfaces. These methods have since been successfully applied in diverse areas such as computer graphics, medical image segmentation and crystal growth [40–42].

We introduce a second field variable  $\chi(\mathbf{r}, \tau)$  which evolves in (virtual) time  $\tau$  according to the so-called reinitialization equation [40, 43, 44]

$$a\partial_\tau\chi + \text{sign}(\chi^0)(|\nabla\chi| - 1) = 0 \quad (21)$$

with

$$\text{sign}(x) = \begin{cases} 1 & \text{if } x > 0 \\ 0 & \text{if } x = 0 \\ -1 & \text{if } x < 0. \end{cases} \quad (22)$$

Equation (21) is solved with the initial condition

$$\chi(\mathbf{r}, 0) = \chi^0(\mathbf{r}) = u(\mathbf{r}, t) - u_c, \quad (23)$$

where  $u_c$  is the activator value along the iso-concentration line  $\gamma$  for which we want to determine the curvature  $\kappa$ , i.e.,  $u(\gamma(s, t), t) = u_c$ . Note that

$$\chi(\gamma(s, t), \tau) = \chi^0(\gamma(s, t)) = 0 \quad (24)$$

for all times  $\tau$  such that the position of the level set  $\gamma$  is not changed by equation (21). However, equation (21) transforms the neighborhood of  $\chi = 0$  such that, after sufficiently many time steps  $\tau$ ,

$$\lim_{\tau \rightarrow \infty} |\nabla\chi(\mathbf{r}, \tau)| = 1. \quad (25)$$

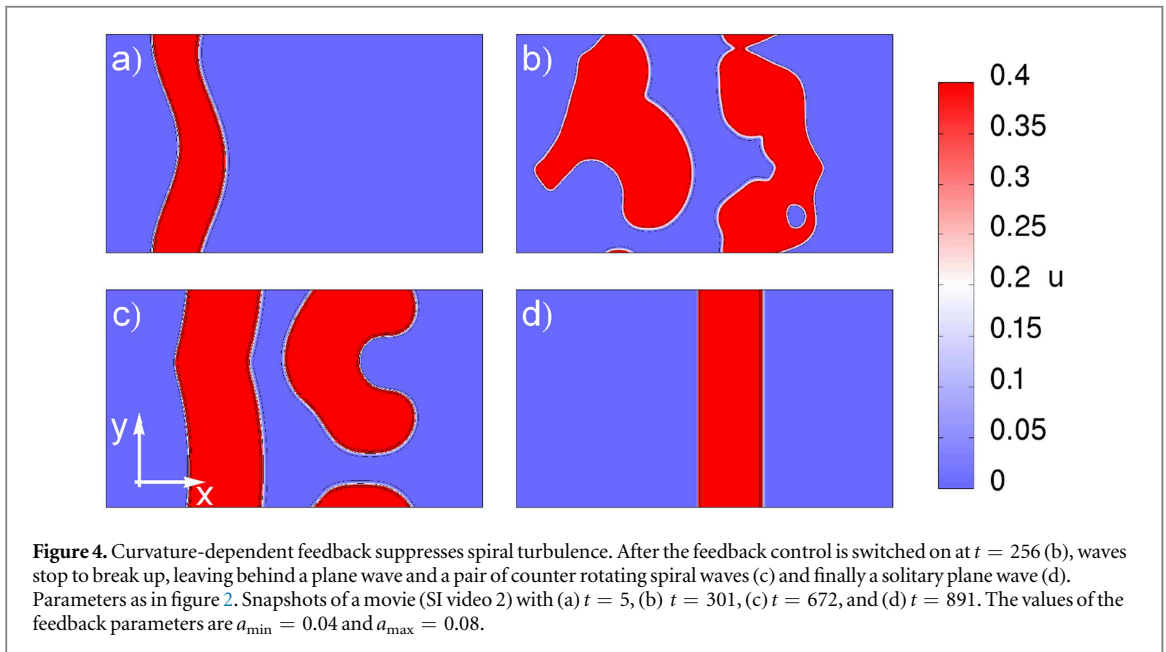
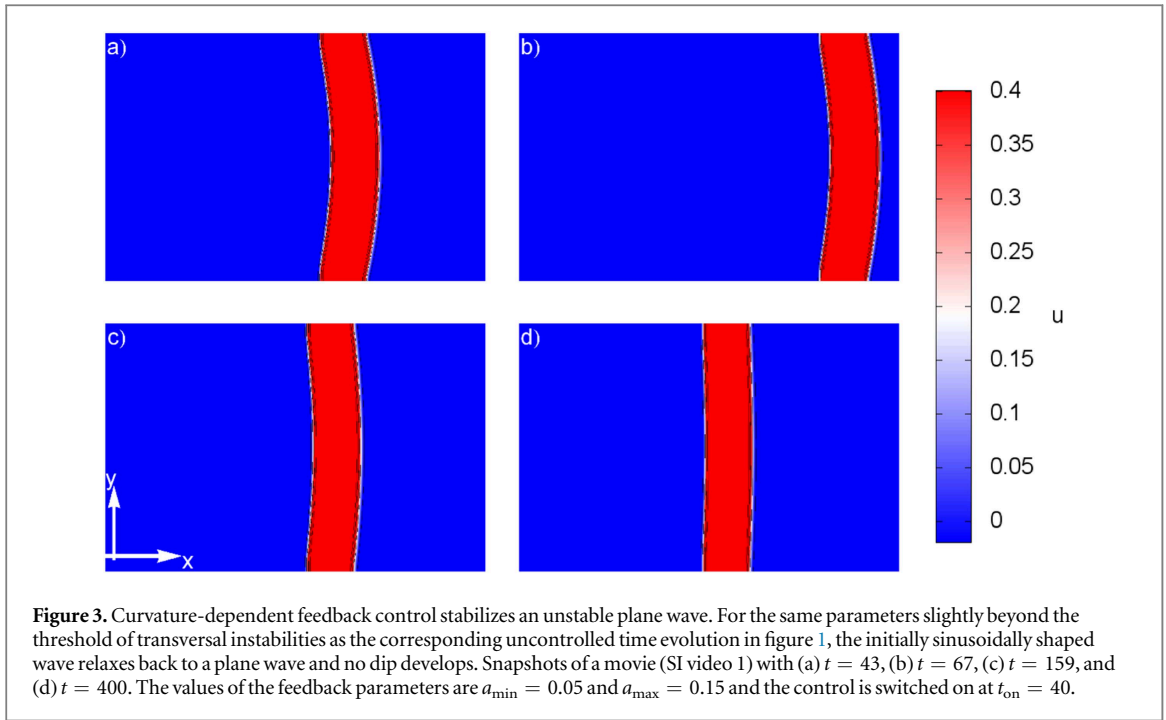
The curvature  $\kappa$  of  $\gamma$ , equation (12) can now readily be computed in terms of the Laplacian of  $\chi$  as

$$\kappa(s, t) = \tilde{\kappa}(\gamma(s, t), t) = \lim_{\tau \rightarrow \infty} \Delta\chi(\gamma(s, t), \tau). \quad (26)$$

Numerically, the evolution of  $\chi$  up to the final time  $\tau = 0.01$  is sufficient to obtain a very accurate smooth result for the curvature of  $\gamma$ . The reinitialisation equation (21) has to be solved at every real time step  $t$ . However, because the time evolution of the RD system is slow enough, we recompute the curvature  $\kappa$  only every 200 time steps.

## 2.5. Results

Figure 3 demonstrates the suppression of a transversal instability. For the same parameter values slightly beyond the threshold as in figure 1, the initially sinusoidally shaped wave relaxes back to a plane wave and no dip appears, see also the video in the supplemental material (SI video 1). Patterns deep in the regime of transversal instabilities are characterized by a continuing segmentation of waves and spreading spiral turbulence as shown in figure 2. For the same parameter values, patterns stop to segment after the feedback is switched on, giving rise to a persistent plane wave and two counter-rotating spiral waves, see figure 4 and the video in the supplemental material (SI video 2). The wave front of rotating patterns has positive curvature. According to the linear eikonal



equation (10), it advances slower than a plane wave if the effective curvature coefficient  $\tilde{\nu}$  is positive. Therefore, the plane wave has a tendency to annihilate rotating waves, which ultimately leads to a single plane wave.

### 3. Excitation of transversal instabilities

#### 3.1. The modified Oregonator model

The modified Oregonator model [45] describes the light-sensitive BZ reaction:

$$\frac{\partial u}{\partial t} = \frac{1}{\epsilon} [u - u^2 + w(q - u)] + D_u \Delta u, \quad (27)$$

$$\frac{\partial v}{\partial t} = u - v, \quad (28)$$



$$\frac{\partial w}{\partial t} = \frac{1}{\tilde{\epsilon}}[\Phi + fv - w(u + q)] + D_w \Delta w. \quad (29)$$

Parameters  $\epsilon$  and  $\tilde{\epsilon}$  characterize the time scales for the dynamics of the activator  $u$  and inhibitor  $w$ , respectively. The stoichiometric parameters  $q$  and  $f$  depend on the temperature and chemical composition. All parameter values used in numerical simulations are listed in table A2 in appendix A. In experiments, the catalyst  $v$  can be immobilized in a gel and therefore the corresponding diffusion coefficient is set to zero. The activator  $u$  and inhibitor  $w$  diffuse with diffusion coefficients  $D_u$  and  $D_w$ , whose ratio for typical BZ recipes is approximately  $D_w/D_u \approx 1.2$  [46]. This value is too low to support transversal instabilities. The parameter  $\Phi$  in equation (29) is proportional to the applied light intensity and the local excitation threshold.

### 3.2. The Kuramoto–Sivashinsky (KS) equation

Apart from nonlinear eikonal equations, which are difficult to solve numerically, patterns arising beyond the threshold of transversal instability can be described by the KS equation [7, 47],

$$\partial_t \phi(y, t) = c + \frac{c}{2}(\partial_y \phi(y, t))^2 + \nu \partial_y^2 \phi(y, t) - \lambda \partial_y^4 \phi(y, t). \quad (30)$$

Equation (30) is an evolution equation for the  $x$ -component  $\phi(y, t)$  of an iso-concentration line  $\gamma$  parametrized in the form  $\gamma(y, t) = (\phi(y, t), y)^T$  (see figure 1). A derivation of equation (30) from a general RD system is given in references [14, 48]. With Neumann boundary conditions at the top and bottom edge of the domain iso-concentration lines of activator and inhibitor meet the domain boundary orthogonally. This corresponds to Neumann boundary conditions for  $\phi$ ,

$$\partial_y \phi(0, t) = 0, \quad \partial_y \phi(L, t) = 0. \quad (31)$$

Similarly, periodic boundary conditions in the RD system carry over to periodic boundary conditions for  $\phi$ . Equation (30) was originally proposed by Sivashinsky [7] in the study of turbulent flame propagation and adapted for reaction-diffusion systems by Kuramoto [14, 47]. The parameter  $\lambda$  can be expressed in terms of a sum over all eigenfunctions of the linear stability operator arising through a linearisation of the one-dimensional RD system around the traveling wave solution [14]. To compute  $\lambda$ , we use a method which avoids the virtually impossible task of computing all eigenfunctions, see [48] for details. The values of  $\lambda$  and  $\nu$  for the modified Oregonator model with parameters as given in appendix A are

$$\lambda = 0.68, \quad \nu = 1.05. \quad (32)$$

The KS equation (30) allows a refined investigation of the onset of transversal instabilities. For a stability analysis of a plane wave in a channel of width  $L$  with Neumann boundary conditions, we apply a perturbation expansion in  $0 < \hat{\epsilon} \ll 1$  with an ansatz in form of a Fourier series,

$$\phi(y, t) = ct + \hat{\epsilon} \sum_{n=-\infty}^{\infty} a_n \exp(\omega_n t) \cos\left(\frac{\pi n y}{L}\right), \quad (33)$$

where  $ct$  corresponds to a plane wave solution of the RD system traveling in  $x$ -direction. The dispersion relation follows as

$$\omega_n = -\lambda \left(\frac{n\pi}{L}\right)^4 - \nu \left(\frac{n\pi}{L}\right)^2. \quad (34)$$

Transversal instabilities occur only if  $\omega_1 > 0$ . This is the case if  $\nu$  is negative and the channel width exceeds

$$L = \pi \sqrt{\frac{\lambda}{-\nu}}. \quad (35)$$

Thus, the transversal instability can be suppressed in thin channels. It is a long-wavelength instability, i.e., the first mode which becomes unstable upon reaching the threshold is the mode with the longest possible wavelength.

As can be seen from equation (35), if  $\nu < 0$ , the fourth order term with  $\lambda > 0$  in the KS equation (30) counteracts the negative diffusion term and leads to a saturation of the growth of wavefront modulations. Starting at the threshold of instability, the solution to the KS equation (30) displays a wave front with a dip located at  $y = L/2$ , similar to the wave pattern shown in figure 1. Upon increasing  $L$ , this steady wave loses stability via a supercritical Hopf bifurcation [15] and the wave front starts to oscillate back and forth in a symmetrical fashion. Increasing  $L$  even further leads to a symmetry breaking bifurcation with asymmetrical oscillations followed by a period doubling cascade to fully developed spatio-temporal chaos. In this regime, the KS equation displays a sensitive dependence on initial conditions. Small variations in the initial state lead to a dramatically different time evolution. This behavior of the KS equation is also studied as an analogy for hydrodynamic turbulence [49].

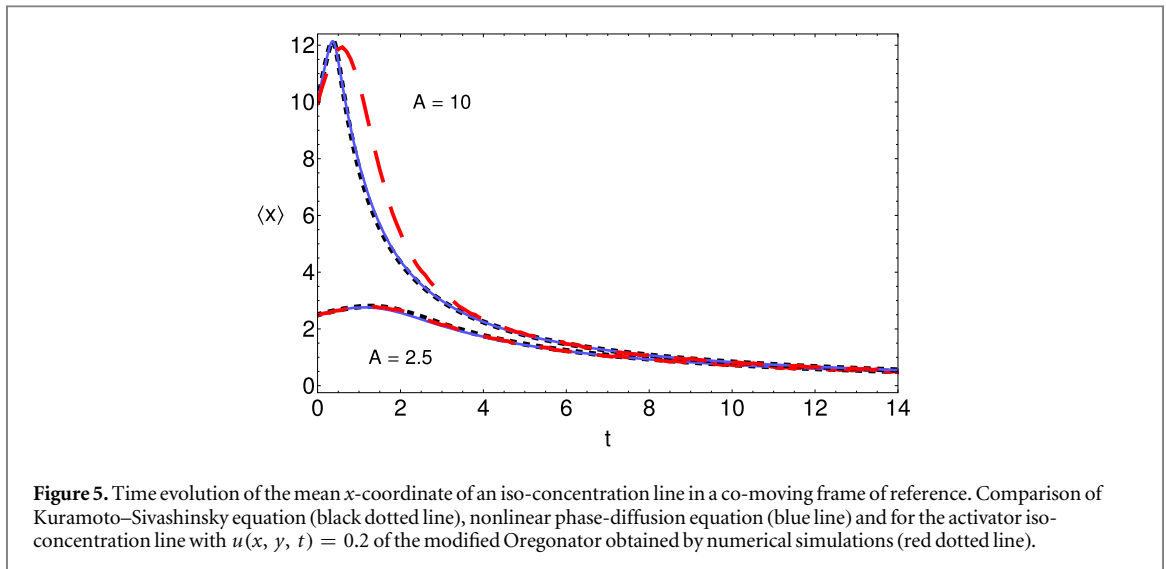


**Figure 5.** Time evolution of the mean  $x$ -coordinate of an iso-concentration line in a co-moving frame of reference. Comparison of Kuramoto–Sivashinsky equation (black dotted line), nonlinear phase-diffusion equation (blue line) and for the activator iso-concentration line with  $u(x, y, t) = 0.2$  of the modified Oregonator obtained by numerical simulations (red dotted line).

As long as  $\nu > 0$ , no instability can arise and the fourth order term can be safely neglected by setting  $\lambda = 0$ . In this case, equation (30) simplifies to the nonlinear phase diffusion equation, which in turn can be transformed to the usual diffusion equation via the Cole–Hopf transform [13]. Therefore, equation (30) with  $\lambda = 0$  can be solved analytically for arbitrary initial and boundary conditions.

To assess the accuracy of the KS equation (30) as an approximation for propagating reaction-diffusion waves, we compare the transition from an initially curved shape to a plane wave for  $\nu > 0$  with numerical simulations of the underlying two-dimensional modified Oregonator model equations (27)–(29). The iso-concentration line  $\gamma$  of the activator variable  $u$  is determined numerically as the set of points  $\mathbf{r} = (x, y)^T$  for which  $u(\mathbf{r}, t) = u_c = 0.2$ . We compute the mean  $x$ -component of the iso-concentration line in a co-moving frame as

$$\langle x \rangle(t) = \frac{1}{L} \int_0^L \phi(y, t) dy - \phi(0, t). \quad (36)$$

Figure 5 shows the time evolution of  $\langle x \rangle(t)$  obtained from the KS equation (black dotted line) and nonlinear phase diffusion equation (blue solid line) and for the modified Oregonator model obtained by numerical simulations (red dashed line) for two different values of the amplitude  $A$  which characterizes the initial deviation from a plane wave. As one would expect intuitively, the agreement between numerical simulations on the one hand and KS equation and nonlinear phase diffusion equation on the other hand becomes worse the larger is the initial amplitude  $A$ . For large times, i.e., when the curved iso-concentration line approaches a straight line, all results agree. The nonlinear phase diffusion equation and the KS equation practically yield the same result for all times. This confirms the fact that the fourth order derivative in the KS equation can safely be neglected if the curvature coefficient is  $\nu > 0$ .

### 3.3. Curvature-dependent feedback control

For the modified Oregonator model, we use the parameter  $\Phi$  as the feedback parameter. A numerical computation of the dependence of the plane wave velocity  $c$  on  $\Phi$  is shown in figure 6. The dependence follows roughly a linear relationship,

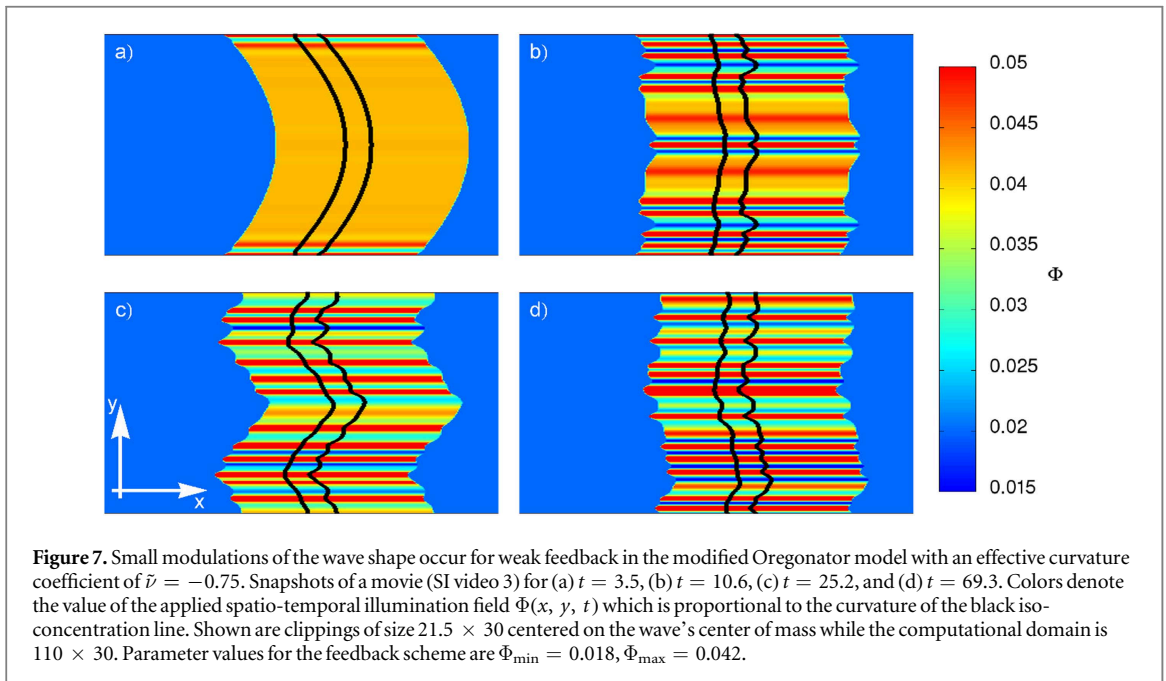
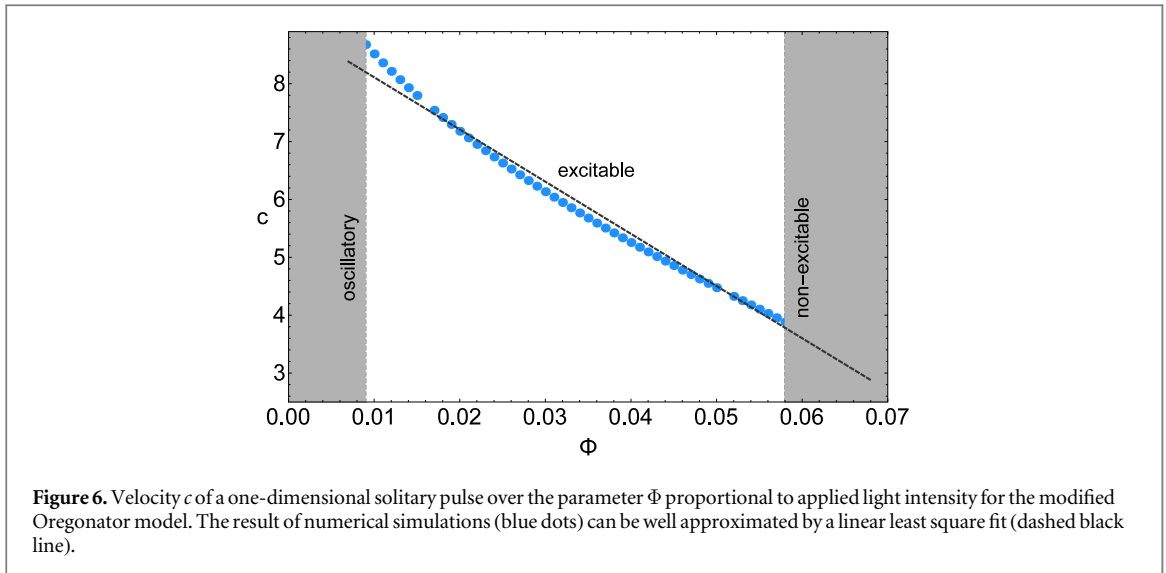
$$c(\Phi) = c_0 + c_1 \Phi, \quad (37)$$

with parameters  $c_1 = -90.191$ ,  $c_0 = 9.013$  obtained from a least square fit. Solitary waves exist only in the excitable regime, which is bounded by dashed lines in figure 6. Below  $\Phi \approx 0.045$ , the rest state is unstable and the medium becomes oscillatory. For  $\Phi \gtrsim 0.068$ , the solitary pulse profile becomes unstable and decays to the stable rest state. A successful feedback control is possible if  $\Phi$  is restricted to lie between these two values. The feedback law for  $\Phi$  depends linearly on the curvature,

$$\Phi(\kappa) = \alpha + \beta \kappa. \quad (38)$$

For the parameters of the feedback scheme we set  $\alpha = \Phi_{\max}$  and  $\beta = -(\Phi_{\max} - \Phi_{\min})/\kappa_{\text{norm}}$  such that the effective curvature coefficient is

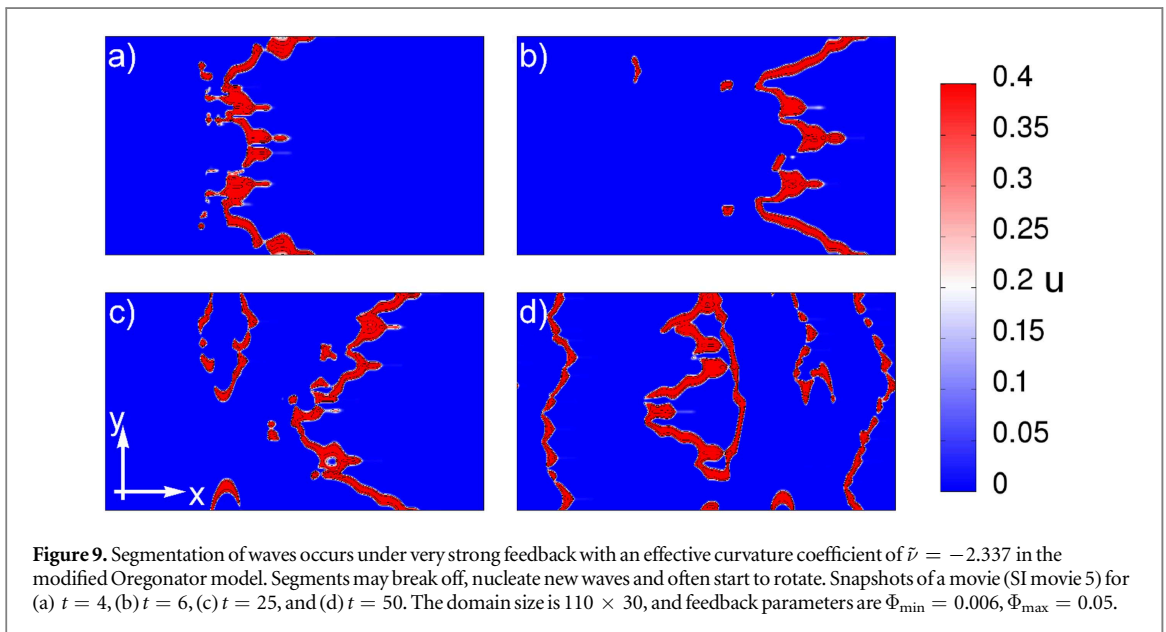
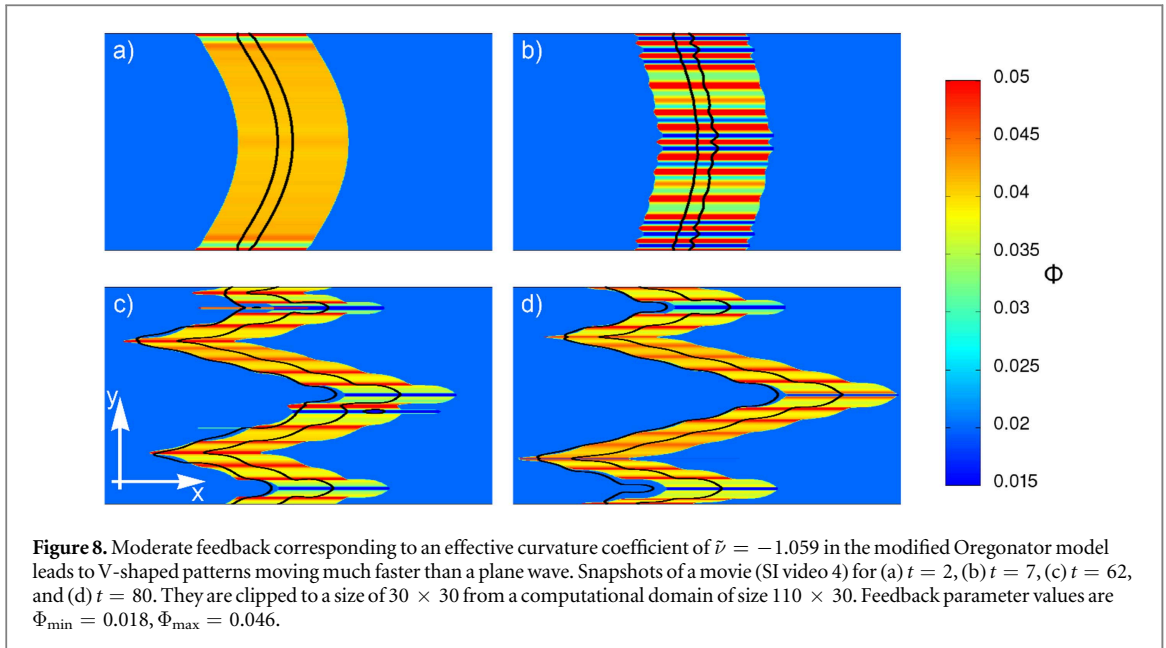
$$\tilde{\nu} = \nu - c_1 \beta = \nu + \frac{c_1}{\kappa_{\text{norm}}} (\Phi_{\max} - \Phi_{\min}). \quad (39)$$



The values of  $\Phi_{\max}$  and  $\Phi_{\min}$  can be chosen arbitrarily as long as  $\Phi_{\min} < \Phi_{\max}$  and both values lie within the regime of an excitable medium, see figure 6. The curvature  $\kappa$  is determined for the activator iso-concentration line  $\gamma$  with  $u(\gamma(s, t), t) = u_c = 0.2$ . An area of fixed size in the front and back of  $\gamma$  is illuminated with the same value  $\Phi(\kappa(s, t))$ , while within the remaining medium  $\Phi$  attains its background value  $\Phi = \Phi_0$ . Before the feedback is switched on at time  $t_1 = 0.4$ , the wave evolves uncontrolled. The value of  $\kappa_{\text{norm}} = 1.2$  is an estimate of the largest value which the curvature attains during the overall time evolution. For simplicity, we choose a constant value of  $\kappa_{\text{norm}}$ , but in principle this value can be set to the maximum curvature every time the curvature is recomputed.

### 3.4. Results

Figure 7 shows wave patterns arising for weak feedback with an effective curvature coefficient  $\tilde{\nu} = -0.75$ , see also the video in the supplemental material (SI video 3). The black solid lines denote the iso-concentration line  $\gamma$  for the activator level  $u_c = 0.2$ . The rightmost line corresponds to the wave front while the trailing line corresponds to the wave back. The colors represent the value of the feedback parameter  $\Phi$  and are proportional to the curvature of the wave front iso-concentration line. An initially sinusoidal shape decays and a plane wave with transversal modulations of small wavelength develops. For the example presented here, the modulations are not stationary but travel along the iso-concentration line until they annihilate each other or at the Neumann



boundaries. For even weaker feedback, the modulations do not travel such that the pattern is truly stationary in a co-moving frame of reference. The overall velocity of the patterns is approximately the velocity  $c$  of the one-dimensional unperturbed traveling wave. Apart from the wavelength of the modulations, this type of pattern is similar to the patterns arising in the uncontrolled FHN model slightly beyond the threshold of transversal instabilities, see figure 1.

Figure 8 displays the effects of moderate feedback with an effective curvature coefficient  $\tilde{\nu} = -1.059$ , see also the video in the supplemental material (SI video 4). V-shaped patterns arise which travel much faster than a corresponding one-dimensional solitary pulse. In a frame of reference co-moving with the center of mass, the V-shaped patterns appear stationary apart from modulations traveling along the iso-concentration line. The V-patterns observed under feedback are long-time stable and do not decay or break up. A solitary V-pattern in an unbounded domain can be explained analytically as a solution to the linear and nonlinear eikonal equations [50, 51]. A V with opening angle  $\alpha$  has a mean velocity  $\tilde{\nu}$  given by

$$\tilde{\nu} = \frac{c}{\sin(\alpha)}, \quad (40)$$

where  $c$  is the one-dimensional velocity. Because  $|\sin(\alpha)| < 1$ , all V-patterns are moving faster than a plane wave. Experimentally, these patterns were observed in homogeneous [52] and stratified [53] BZ media.

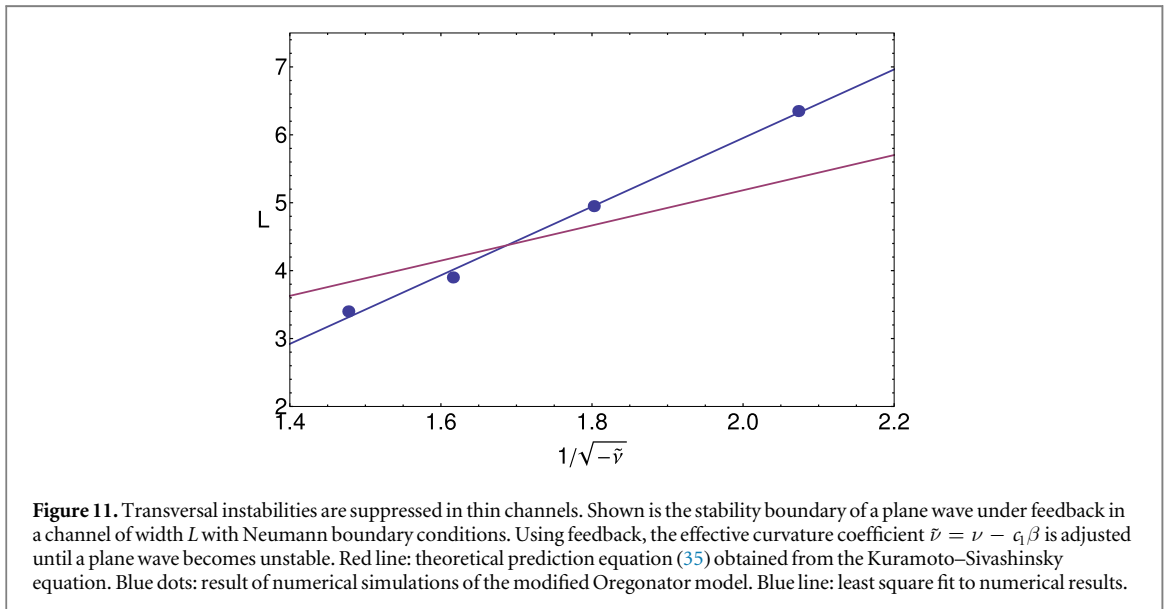
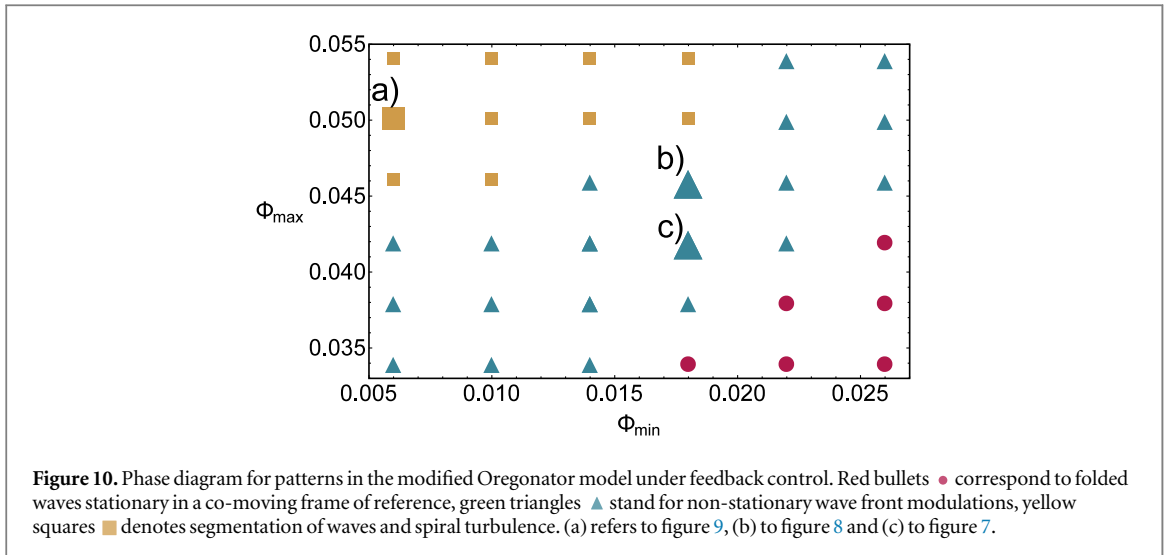
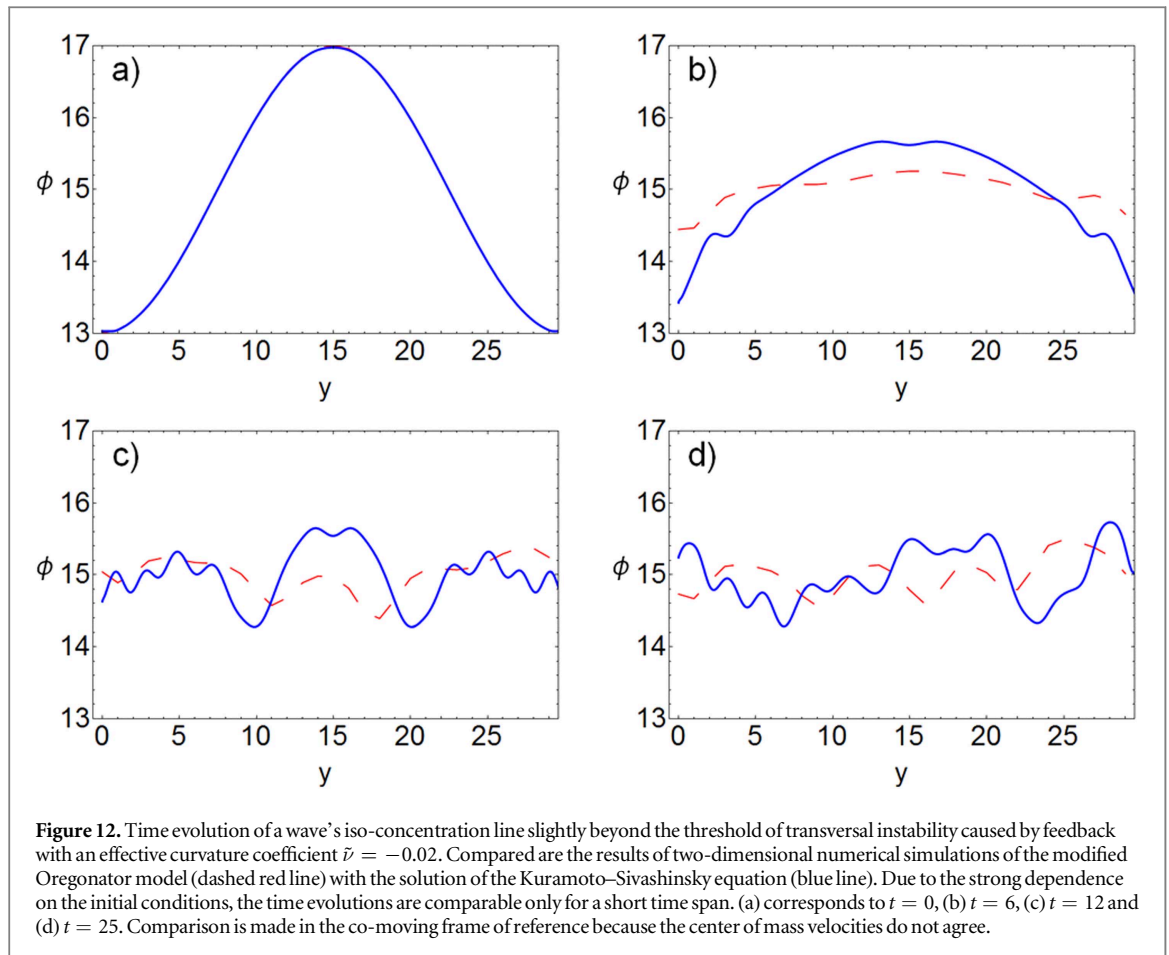


Figure 9 shows the effect of strong feedback with an effective curvature coefficient  $\tilde{\nu} = -2.337$ , see also the video in the supplemental material (SI video 5). Similar as for moderate feedback, V-shaped patterns appear. However, their shape is non-stationary and oscillating. The V-shape is segmented in an irregular and non-stationary way, with segments either merging again or breaking off and serving as the nucleation site for new waves. These new waves propagate as segmented circles and occasionally start to rotate until they annihilate upon collision with other waves. Qualitatively, the segmentation and occurrence of rotating segments is similar to the spreading spiral turbulence observed for the uncontrolled FHN model deep in the regime of transversal instabilities, see figure 2.

These results show that the proposed feedback scheme is not only able to excite transversal instabilities but allows, to some extent, the selection of patterns beyond the instability threshold by tuning the feedback parameters  $\Phi_{\max}$  and  $\Phi_{\min}$ , which are accessible to an experimentalist. We present a phase diagram with a classification of the observed patterns in the  $\Phi_{\max} - \Phi_{\min}$  plane in figure 10. Note that according to the KS equation (30), the observed patterns should only depend on the effective curvature coefficient  $\tilde{\nu}$  given by equation (39). However, numerical simulations show that the type of pattern depends not only on the difference of  $\Phi_{\max}$  and  $\Phi_{\min}$ , but also displays a slight dependence on their absolute values. This dependence is due to nonlinear corrections in the relation for the one-dimensional velocity  $c$  over  $\Phi$  and higher order effects neglected by the KS equation (30). By adjusting the effective curvature coefficient  $\tilde{\nu}$ , we are able to validate the predicted onset of transversal instabilities equation (35),

$$L = \pi \sqrt{\frac{\lambda}{-\tilde{\nu}}} \quad (41)$$



and its dependence on the channel width  $L$ . We perform numerical simulations of the controlled Oregonator model in a channel with width  $L$  and Neumann boundary conditions in the  $y$ -direction. Starting from a planar noisy wavefront (7), we change the effective curvature coefficient  $\tilde{\nu}$  until a plane wave becomes unstable, i.e., the curvature along the iso-concentration line is different from zero. Figure 11 shows that both numerical simulations and analytical prediction yield a linear relation between channel width  $L$  and  $1/\sqrt{-\tilde{\nu}}$  over a large range of effective curvature coefficients  $\tilde{\nu}$ . The slopes differ due to higher order corrections for the KS equation (30) and nonlinear corrections for the velocity  $c$  over  $\Phi$ , equation (37), used for the feedback scheme.

Beyond the onset of transversal instabilities, the emerging patterns can in principle be described by the KS equation (30). We compare the time evolution of the modified Oregonator model with the solution of the KS equation for an effective curvature coefficient of  $\tilde{\nu} = -0.02$  (figure 12). Due to sensitive dependence on initial data, any early agreement between the two curves vanishes quickly during time evolution.

#### 4. Conclusions

In this article, we present a feedback loop to induce, control, and suppress transversal instabilities of reaction-diffusion waves. The control signal is calculated from the local curvature of the iso-concentration line of the wave. We show that the curvature-dependent control can amplify or suppress small curvature perturbations in the wave shape. Simultaneously, the feedback allows one to study a large variety of artificially produced wave patterns associated with transversal instabilities. Often these patterns are non-stationary and sensitively depend on small changes in the initial conditions, which is a characteristic of chaotic dynamics.

Mathematically, the onset of transversal instabilities can be understood with the help of the linear eikonal equation, which relates the wave velocity normal to an iso-concentration line to its local curvature. The coefficient  $\nu$  in front of the curvature determines the stability of a flat wave. For positive values of  $\nu$ , convex wave segments slow down while concave wave segments propagate at a higher velocity. Under these conditions a perturbed flat traveling wave recovers its flat shape. In the case of negative  $\nu$ , a small positive curvature causes an increase of the wave velocity, which in turn increases the local curvature. Now, a flat wave is unstable with respect to small curvature perturbations. The proposed feedback loop allows for finely tuning and changing the sign of the coefficient  $\nu$ .

With experiments on chemical waves in the PBZR in mind, for realistic parameter values we show in numerical simulations with the Oregonator model that transversal instabilities of planar waves can be induced by the feedback. Right beyond the transversal instability of planar waves, we find nearly flat folded waves which are stationary in a co-moving frame of reference. For weak feedback we observe small ripple-shaped undulations traveling along the wave front. Upon increasing the feedback strength further, V-shaped wave patterns with spatio-temporal transversal modulations appear. These V-shaped waves travel at a velocity that depends on the opening angle but is considerably faster than that of the planar wave. Far away from the instability threshold, breakup of waves causes persistent annihilation and merging of excited domains, self-sustained rotational motion and nucleation of rotating wave segments. Qualitatively, the emerging wave patterns correspond to those observed in numerical simulations with separated activator and inhibitor diffusivity [12].

Regarding chemical wave propagation in the PBZR, we emphasize that the feedback parameters of the control scheme are experimentally accessible. For suitable BZ concentrations the dependence of the wave velocity on the intensity of applied light should be strong enough to induce transversal wave instabilities. The iso-concentration line of the wave can be determined by 2d spectrophotometry with sufficient spatial resolution using the contrast between oxidized and reduced form of the catalyst. We expect that computation of the curvature by the Level Set Method as described in section 2.4 will work reliably for noisy experimental data, too. Because all chemical components share similarly shaped iso-concentration lines, the measurement of the concentration field of an arbitrary single chemical species is sufficient for setting up the control loop. Fine-tuning the feedback parameters allows one to study the onset of transversal instabilities in dependence of the boundary conditions as e.g. the channel width  $L$ , as pointed out in section 2.2.

In the opposite case, sufficiently strong feedback changes the sign of the effective curvature coefficient from negative to positive. Consequently, naturally occurring transversal wave instabilities leading to the breakup of waves are suppressed—the feedback stabilizes planar waves and spiral waves. Spreading of spiral turbulence is inhibited due to the suppression of segmentation of waves.

Reaction-diffusion waves describe, at least approximately, a huge variety of wave processes in biology. Our results are potentially applicable to deliberately induce or inhibit transversal wave instabilities and to control the emerging patterns under very general conditions. The essential condition for applicability is that the propagation velocity of the wave can be externally controlled over a sufficiently large range such that the curvature coefficient of the eikonal equation switches its sign.

Moreover, we expect that curvature dependent feedback might have interesting applications in interfacial pattern formation. For example, this feedback mechanism could be the starting point for a control strategy aimed at the purposeful selection of patterns affected by instabilities as in, e.g., bacterial colony growth [54], dendrite formation in batteries [55] or alloys growing into an undercooled melt [56, 57].

## Acknowledgments

We acknowledge helpful discussions with Matthew Henessy and Frédéric Gibou as well as financial support from the German Science Foundation (DFG) within the GRK 1558 (ST, JL, JFT) and within the framework of Collaborative Research Center 910 (JFT and HE).

## Appendix A. Parameter values for numerical simulations

**Table A1.** Parameter values used for numerical simulations of the piecewise linear FitzHugh–Nagumo model.

Parameter	Value	Description
$a$	0.1	Excitation threshold
$k_f$	2	Model parameter
$k_g$	2	Model parameter
$\sigma$	2.1	Ratio of diffusion coefficients
$\delta$	0.01	Model parameter
$\epsilon$	0.1425	Time scale separation
$c_1$	−8.75	Slope of linear fit for velocity over $a$
$c_0$	2.23	Constant of linear fit for velocity over $a$
$\Delta t$	0.00001	Time step
$\Delta x, \Delta y$	0.15	Step width of spatial resolution

**Table A2.** Parameter values used for numerical simulations of the modified Oregonator model.

Parameter	Value	Description
$f$	1.4	Stoichiometric parameter
$q$	0.002	Model parameter
$\epsilon$	1/49	Time scale separation
$\tilde{\epsilon}$	1/4410	Time scale separation
$\Phi_0$	0.02	Background illumination
$D_u$	1.0	Activator diffusion coefficient
$D_w$	1.2	Inhibitor diffusion coefficient
$\nu$	1.05	Curvature coefficient
$\lambda$	0.68	Fourth order coefficient in the KS equation
$c_1$	-90.19	Slope of linear fit for velocity over $\Phi$
$c_0$	9.01	Constant of linear fit for velocity over $\Phi$
$\kappa_{\text{norm}}$	1.2	Curvature normalization
$\Delta t$	0.0001	Time step
$\Delta x, \Delta y$	0.05	Step width of spatial resolution

## Appendix B. Bonnet's formula

We prove the formula of Bonnet, i.e., we demonstrate that evaluating the curvature field defined by equation (19) at an iso-concentration line  $\gamma$  yields the curvature of  $\gamma$ . We write

$$\partial_x u(x, y) |_{x=\gamma_x(y)} = \partial_x u(\gamma_x(y), y) \quad (\text{B.1})$$

for derivatives with respect to  $x$ . Let  $u = u(x, y)$  be the map  $\mathbb{R}^2 \rightarrow \mathbb{R}$  and  $\gamma(y) = (\gamma_x(y), y)^T$  be the iso-concentration line  $\gamma$  parametrized by  $y$ . It follows that  $u(\gamma_x(y), y) = u_c = \text{const.}$  for all values of  $y$ . Therefore we can write

$$\frac{d}{dy} u(\gamma_x(y), y) = \partial_x u(\gamma_x(y), y) \gamma'_x(y) + \partial_y u(\gamma_x(y), y) = 0 \quad (\text{B.2})$$

and

$$\begin{aligned} \frac{d^2}{dy^2} u(\gamma_x(y), y) &= \frac{d}{dy} (\partial_x u(\gamma_x(y), y) \gamma'_x(y) + \partial_y u(\gamma_x(y), y)) \\ &= \partial_x u(\gamma_x(y), y) \gamma''_x(y) + \partial_x^2 u(\gamma_x(y), y) (\gamma'_x(y))^2 \\ &\quad + 2\partial_y \partial_x u(\gamma_x(y), y) \gamma'_x(y) + \partial_y^2 u(\gamma_x(y), y) \\ &= 0 \end{aligned} \quad (\text{B.3})$$

and generally  $\frac{d^n}{dy^n} u(\gamma_x(y), y) = 0$  with  $n \in \mathbb{N}$ ,  $n > 0$ . The curvature field  $\tilde{\kappa}$ , equation (19), expressed in Cartesian coordinates is

$$\begin{aligned} \tilde{\kappa}(x, y) &= \frac{\partial_y^2 u(x, y) (\partial_x u(x, y))^2 - 2\partial_x u(x, y) \partial_y u(x, y) \partial_{x,y} u(x, y)}{((\partial_x u(x, y))^2 + (\partial_y u(x, y))^2)^{3/2}} \\ &\quad + \frac{\partial_x^2 u(x, y) (\partial_y u(x, y))^2}{((\partial_x u(x, y))^2 + (\partial_y u(x, y))^2)^{3/2}}. \end{aligned} \quad (\text{B.4})$$

Evaluating  $\tilde{\kappa}$  at the iso-concentration line yields

$$\begin{aligned} \tilde{\kappa}(\gamma_x(y), y) &= \frac{\partial_y^2 u(\gamma_x(y), y) (\partial_x u(\gamma_x(y), y))^2 + \partial_x^2 u(\gamma_x(y), y) (\partial_y u(\gamma_x(y), y))^2}{((\partial_x u(\gamma_x(y), y))^2 + (\partial_y u(\gamma_x(y), y))^2)^{3/2}} \\ &\quad - \frac{2\partial_x u(\gamma_x(y), y) \partial_y u(\gamma_x(y), y) \partial_{x,y} u(\gamma_x(y), y)}{((\partial_x u(\gamma_x(y), y))^2 + (\partial_y u(\gamma_x(y), y))^2)^{3/2}}. \end{aligned} \quad (\text{B.5})$$

Using equation (B.2), the denominator of equation (B.5) can be simplified as

$$\begin{aligned} (\partial_x u(\gamma_x(y), y))^2 + (\partial_y u(\gamma_x(y), y))^2 &= (\partial_x u(\gamma_x(y), y))^2 + (-\partial_x u(\gamma_x(y), y) \gamma'_x(y))^2 \\ &= (\partial_x u(\gamma_x(y), y))^2 (1 + (\gamma'_x(y))^2). \end{aligned} \quad (\text{B.6})$$



Similarly, using equations (B.2) and (B.3), the first term of the numerator of equation (B.5) can be rewritten in the form

$$\begin{aligned} \partial_y^2 u(\gamma_x(y), y) (\partial_x u(\gamma_x(y), y))^2 &= -(\partial_x u(\gamma_x(y), y))^2 (\partial_x u(\gamma_x(y), y) \gamma_x''(x) \\ &+ \partial_x^2 u(\gamma_x(y), y) (\gamma_x'(x))^2 + 2\partial_{x,y} u(\gamma_x(y), y) \gamma_x'(y)), \end{aligned} \quad (\text{B.7})$$

while the second term of the numerator of equation (B.5) can be cast as

$$\partial_x^2 u(\gamma_x(y), y) (\partial_y u(\gamma_x(y), y))^2 = \partial_x^2 u(\gamma_x(y), y) (\partial_x u(\gamma_x(y), y))^2 (\gamma_x'(x))^2. \quad (\text{B.8})$$

The last term of the numerator of equation (B.5) becomes

$$\begin{aligned} &- 2\partial_x u(\gamma_x(y), y) \partial_y u(\gamma_x(y), y) \partial_{x,y} u(\gamma_x(y), y) \\ &= 2(\partial_x u(\gamma_x(y), y))^2 \partial_{x,y} u(\gamma_x(y), y) \gamma_x'(y). \end{aligned} \quad (\text{B.9})$$

All terms except the term proportional to  $\gamma_x''(x)$  in the numerator cancel. We are left with

$$\tilde{\kappa}(\gamma_x(y), y) = -\frac{\gamma_x''(y)}{(1 + (\gamma_x'(y))^2)^{3/2}}, \quad (\text{B.10})$$

which is exactly the curvature of a graph, see equation (12).

## ORCID iDs

Jan Frederik Totz  <https://orcid.org/0000-0003-4961-1630>

## References

- [1] Langer J S 1980 Instabilities and pattern formation in crystal growth *Rev. Mod. Phys.* **52** 1
- [2] Langer J S 1989 Dendrites, viscous fingers, and the theory of pattern formation *Science* **243** 1150
- [3] Brenner E and Mel'nikov V 1991 Pattern selection in two-dimensional dendritic growth *Adv. Phys.* **40** 53
- [4] Saffman P G and Taylor G 1958 The penetration of a fluid into a porous medium or Hele–Shaw cell containing a more viscous liquid *Proc. R. Soc. A* **245** 312
- [5] van Saarloos W 1998 Three basic issues concerning interface dynamics in nonequilibrium pattern formation *Phys. Rep.* **301** 9
- [6] De Wit A and Homayouni G M 1999 Viscous fingering in reaction-diffusion systems *J. Chem. Phys.* **110** 8663
- [7] Sivashinsky G I 1977 Nonlinear analysis of hydrodynamic instability in laminar flames: I. Derivation of basic equations *Acta Astronaut.* **4** 1177
- [8] Barenblatt G 1985 *The Mathematical Theory of Combustion and Explosions* (Berlin: Springer)
- [9] Birikh R V, Briskman V A, Velarde M G and Legros J-C 2003 *Liquid Interfacial Systems: Oscillations and Instability* (Boca Raton, FL: CRC Press)
- [10] Méhes E and Vicsek T 2014 Collective motion of cells: from experiments to models *Integr. Biol.* **6** 831
- [11] Marée A F M and Panfilov A V 1997 Spiral breakup in excitable tissue due to lateral instability *Phys. Rev. Lett.* **78** 1819
- [12] Zykov V S, Mikhailov A S and Müller S C 1998 Wave Instabilities in excitable media with fast inhibitor diffusion *Phys. Rev. Lett.* **81** 2811
- [13] Kuramoto Y 1984 *Chemical Oscillations, Waves, and Turbulence* (Berlin: Springer) (<https://doi.org/10.1007/978-3-642-69689-3>)
- [14] Kuramoto Y 1980 Instability and turbulence of wavefronts in reaction-diffusion systems *Prog. Theor. Phys.* **63** 1885
- [15] Horváth D, Petrov V, Scott S K and Showalter K 1993 Instabilities in propagating reaction-diffusion fronts *J. Chem. Phys.* **98** 6332
- [16] Horváth D and Showalter K 1995 Instabilities in propagating reaction-diffusion fronts of the iodate-arsenous acid reaction *J. Chem. Phys.* **102** 2471
- [17] Horváth D and Tóth Á 1998 Diffusion-driven front instabilities in the chlorite-tetrathionate reaction *J. Chem. Phys.* **108** 1447
- [18] Field R J and Burger M (ed) 1985 *Oscillations and Traveling Waves in Chemical Systems* (New York: Wiley)
- [19] Vanag V and Epstein I 2001 Pattern formation in a tunable medium: the Belousov–Zhabotinsky reaction in an aerosol OT microemulsion *Phys. Rev. Lett.* **87** 228301
- [20] Horváth D, Tóth Á and Yoshikawa K 1999 Electric field induced lateral instability in a simple autocatalytic front *J. Chem. Phys.* **111** 10
- [21] Tóth Á, Horváth D and van Saarloos W 1999 Lateral instabilities of cubic autocatalytic reaction fronts in a constant electric field *J. Chem. Phys.* **111** 10964
- [22] Tóth Á, Horváth D, Jakab É, Merkin J H and Scott S K 2001 Lateral instabilities in cubic autocatalytic reaction fronts: the effect of autocatalyst decay *J. Chem. Phys.* **114** 9947
- [23] Toth R and Taylor A F 2006 The tris(2,2'-bipyridyl)ruthenium-catalysed Belousov–Zhabotinsky reaction *Prog. React. Kinet. Mech.* **31** 59
- [24] Kheowan O-U, Davydov V A, Manz N and Müller S C 2007 Compensation of curvature effects by illumination *Phys. Lett. A* **367** 311
- [25] Sakurai T, Mihaliuk E, Chirila F and Showalter K 2002 Design and control of wave propagation patterns in excitable media *Science* **296** 2009
- [26] Mihaliuk E, Sakurai T, Chirila F and Showalter K 2002 Feedback stabilization of unstable propagating waves *Phys. Rev. E* **65** 065602
- [27] Steinbock O, Zykov V and Müller S C 1993 Control of spiral-wave dynamics in active media by periodic modulation of excitability *Nature* **366** 322
- [28] Zykov V S, Steinbock O and Müller S C 1994 External forcing of spiral waves *Chaos* **4** 509
- [29] Zykov V, Bordiougov G, Brandtstädter H, Gerdes I and Engel H 2004 Global control of spiral wave dynamics in an excitable domain of circular and elliptical shape *Phys. Rev. Lett.* **92** 018304
- [30] Schlesner J, Zykov V, Engel H and Schöll E 2006 Stabilization of unstable rigid rotation of spiral waves in excitable media *Phys. Rev. E* **74** 046215

- [31] Schlesner J, Zykov V S, Brandtstädter H, Gerdes I and Engel H 2008 Efficient control of spiral wave location in an excitable medium with localized heterogeneities *New J. Phys.* **10** 015003
- [32] Zykov V S 1987 *Simulation of Wave Processes in Excitable Media* (Manchester: Manchester University Press)
- [33] Press W H, Teukolsky S A, Vetterling W T and Flannery B P 2007 *Numerical Recipes: The Art of Scientific Computing* (Cambridge: Cambridge University Press)
- [34] Dierckx H, Bernus O and Verschelde H 2011 Accurate eikonal-curvature relation for wave fronts in locally anisotropic reaction-diffusion systems *Phys. Rev. Lett.* **107** 108101
- [35] Zykov V S 1980 Analytic evaluation of the relationship between the speed of a wave of excitation in a two-dimensional excitable medium and the curvature of its front *Biofizika* **25** 888
- [36] Mikhailov A and Zykov V 1991 Kinematical theory of spiral waves in excitable media: comparison with numerical simulations *Physica D* **52** 379
- [37] Zykov V and Engel H 2004 Feedback-mediated control of spiral waves *Physica D* **199** 243
- [38] Molnos S 2014 Krümmungsbedingte Instabilitäten von Reaktions-Diffusionswellen *MSc thesis* TU Berlin, Berlin
- [39] Salamon S, Abbena E and Gray A 1997 *Modern Differential Geometry of Curves and Surfaces with Mathematica* (Boca Raton, FL: CRC Press)
- [40] Osher S and Fedkiw R 2003 *Level Set Methods and Dynamic Implicit Surfaces* (Berlin: Springer) (<https://doi.org/10.1007/b98879>)
- [41] Osher S and Sethian J A 1988 Fronts propagating with curvature-dependent speed: algorithms based on Hamilton–Jacobi formulations *J. Comput. Phys.* **79** 12
- [42] Sethian J A 1999 *Level Set Methods and Fast Marching Methods: Evolving Interfaces in Computational Geometry, Fluid Mechanics, Computer Vision, and Materials Science* (Cambridge: Cambridge University Press)
- [43] Russo G and Smereka P 2000 A remark on computing distance functions *J. Comput. Phys.* **163** 51
- [44] du Chéné A, Min C and Gibou F 2008 Second-order accurate computation of curvatures in a level set framework using novel high-order reinitialization schemes *J. Sci. Comput.* **35** 114
- [45] Krug H J, Pohlmann L and Kuhnert L 1990 Analysis of the modified complete Oregonator accounting for oxygen sensitivity and photosensitivity of Belousov–Zhabotinskii systems *J. Phys. Chem.* **94** 4862
- [46] Brandtstädter H, Braune M, Schebesch I and Engel H 2000 Experimental study of the dynamics of spiral pairs in light-sensitive Belousov–Zhabotinskii media using an open-gel reactor *Chem. Phys. Lett.* **323** 145
- [47] Kuramoto Y 1978 Diffusion-induced chaos in reaction systems *Prog. Theor. Phys. Suppl.* **64** 346
- [48] Malevanets A, Careta A and Kapral R 1995 Biscala chaos in propagating fronts *Phys. Rev. E* **52** 4724
- [49] Cvitanovic P, Artuso R, Mainieri R, Tanner G and Vattay G 2016 *Chaos: Classical and Quantum* (Copenhagen: Chaos Book)
- [50] Brazhnik P K and Davydov V A 1995 Non-spiral autowave structures in unrestricted excitable media *Phys. Lett. A* **199** 40
- [51] Brazhnik P K 1996 Exact solutions for the kinematic model of autowaves in two-dimensional excitable media *Physica D* **94** 205
- [52] Pérez-Muñuzuri V, Gómez-Gesteira M, Muñuzuri A P, Davydov V A and Pérez-Villar V 1995 V-shaped stable nonspiral patterns *Phys. Rev. E* **51** R845
- [53] Steinbock O, Zykov V S and Müller S C 1993 Wave propagation in an excitable medium along a line of a velocity jump *Phys. Rev. E* **48** 3295
- [54] Golding I, Kozlovsky Y, Cohen I and Ben-Jacob E 1998 Studies of bacterial branching growth using reaction-diffusion models for colonial development *Physica A* **260** 510
- [55] Bhattacharyya R, Key B, Chen H, Best A S, Hollenkamp A F and Grey C P 2010 *In situ* NMR observation of the formation of metallic lithium microstructures in lithium batteries *Nat. Mater.* **9** 504
- [56] Lipton J, Glicksman M E and Kurz W 1984 Dendritic growth into undercooled alloy metals *Mater. Sci. Eng.* **65** 57
- [57] Chopra M A, Glicksman M E and Singh N B 1988 Dendritic solidification in binary alloys *Metall. Trans. A* **19** 3087